

Start-up vortex flow past an accelerated flat plate

Ling Xu^{1, a)} and Monika Nitsche^{2, b)}

¹⁾*Department of Mathematics and Statistics, Georgia State University, Atlanta, GA 30303, USA*

²⁾*Department of Mathematics and Statistics, University of New Mexico, Albuquerque, NM 87131, USA*

(Dated: 18 April 2014)

Viscous flow past a finite flat plate moving in direction normal to itself is studied numerically. The plate moves with velocity at^p , where $p = 0, 0.5, 1, 2$. We present the evolution of vorticity profiles, streaklines and streamlines, and study the dependence on the acceleration parameter p . Four stages in the vortex evolution, as proposed by Luchini & Tognaccini (2002), are clearly identified. The initial stage, in which the vorticity consists solely of a Rayleigh boundary layer, is shown to last for a time-interval whose length shrinks to zero like p^3 , as $p \rightarrow 0$. In the second stage, a center of rotation develops near the tip of the plate, well before a vorticity maximum within the vortex core develops. Once the vorticity maximum develops, its position oscillates and differs from the center of rotation. The difference between the two increases with increasing p , and decreases in time. In the third stage, the center of rotation and the shed circulation closely satisfy self-similar scaling laws for inviscid flow. Finally, in the fourth stage, the finite plate length becomes relevant and the flow begins to depart from the self-similar behaviour. While the core trajectory and circulation closely satisfy inviscid scaling laws, the vorticity maximum and the boundary layer thickness follow viscous scaling laws. The results are compared with experimental results of Pullin & Perry (1980), and Taneda & Honji (1971), where available.

Keywords: Starting vortex; power law; viscous flow; separation; Reynolds; streaklines; vortex center

I. INTRODUCTION

This paper presents numerical simulations of the starting vortex flow at the edge of an accelerating finite flat plate. The plate is assumed to have zero thickness, and moves with speed $U(t) = at^p$ in direction normal to itself. The flow is nondimensionalized based on the plate length and the parameter a , yielding a characteristic flow Reynolds number Re . Here we study the effect of the acceleration parameter p for fixed Reynolds number $Re = 500$. The effect of varying Re for fixed p is presented elsewhere¹⁶.

Being of intrinsic interest in fluid dynamics, the starting vortex flow has been the focus of many research works, beginning with the work of Prandtl in 1904^{1,6}. Most relevant to the accelerated case considered here are the following. Taneda & Honji¹³ presented experimental results for both uniform and accelerated flow past a plate, and observed an apparent scaling of the vortex size. Pullin and Perry¹¹ performed experiments of flow past finite wedges, with wedges as small as 5° , which serve as a basis of comparison for our present results. They reported detailed measurements of the vortex core trajectory at early times, and compared their observations to inviscid similarity theory results obtained by Pullin¹⁰. The theory holds for inviscid vortex sheet separation at the edge of a semi-infinite plate. In view of the absence of a plate or viscous length scale, in that

case the vortex center trajectory and the shed circulation satisfy inviscid scaling laws in time that were already reported by Kaden² in 1931. Pullin¹⁰ computed the time-independent self-similar shape using an iterative scheme.

Scaling laws also exist for viscous flow past a semi-infinite plate, and follow from dimensional analysis. However, in this case the solution depends on the viscous length scale. The viscous scaling was exploited by Luchini and Tognaccini⁵, who computed flow past a semi-infinite plate in a self-similar reference frame. The finite plate case was studied numerically by Koumoutsakos and Shields³. They computed flow past a plate moving with either impulsively started velocity or constant acceleration. For their accelerated flow, they observe a shear layer instability similar to that observed by Pierce⁹ and Lian and Huang⁴. These numerical results are given mostly for relatively large times.

Here, we use highly resolved simulations to present a systematic study of the dependence on p over a large range of times. We present the evolution of vorticity profiles, streaklines and streamlines, track vortex core trajectories and vorticities, and compute the shed circulation following the approach taken in Xu and Nitsche¹⁶.

Luchini and Tognaccini⁵ propose four different time regimes for viscous flow past finite plates, and it is interesting to identify these regimes using the present simulations. We observe and present the timescales of an initial Rayleigh flow regime. We study the emergence of a vortex core in a second regime, and compare two possible definitions, namely the center of rotation and the position of the vorticity maximum. We observe the self-similar scaling laws in a third regime, and estimate the time at which the finite plate length dominates, in a

^{a)}Electronic mail: lxu9@gsu.edu

^{b)}Electronic mail: nitsche@math.unm.edu

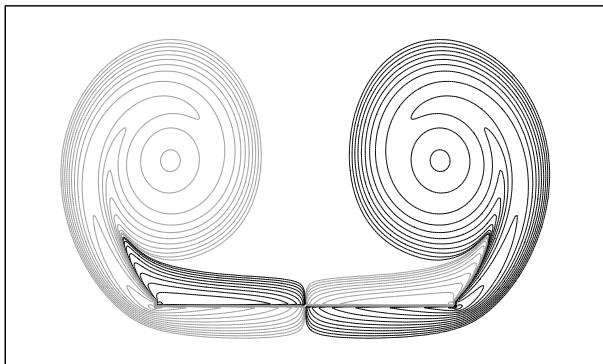


FIG. 1. Sample vorticity contours for $p = 0$ at a relatively large time, with positive vorticity in black, negative vorticity in grey.

fourth regime. All results are computed with $Re = 500$, with the exception of a comparison with experimental results by Pullin and Perry, for which $Re = 6000$, and $p = 0.45$. The results are also compared with the scaling behaviour proposed by Taneda and Honji¹³.

The paper is organized as follows. Sections II and III present the problem and the numerical method used, section IV presents the numerical results, section V summarizes the observations.

II. PROBLEM FORMULATION

A finite plate of length L and zero thickness, immersed in a homogeneous viscous fluid, is accelerated in direction normal to itself with speed

$$\hat{U}(\hat{t}) = a\hat{t}^p, \quad (1)$$

where a is a dimensional constant. Here and throughout the paper, the hat symbol denotes that the variables are dimensional. We consider $p = 0, 0.5, 1, 2$. These include impulsively started flow ($p = 0$), uniform acceleration ($p = 1$), and linear acceleration ($p = 2$). The flow is assumed to be two-dimensional, and to remain symmetric about the centerline at all times. We choose a reference frame fixed on the plate, in which the plate is horizontal and the driving velocity moves upwards, approaching parallel flow in the far field. Figure 1 illustrates the fluid vorticity some time after the beginning of the motion. As fluid moves from upstream (below the plate) to downstream (above the plate), boundary layers of vorticity form along the plate walls which eventually separate and form a pair of counterrotating vortices. We note that changing to an accelerated time-dependent reference frame does not affect the vorticity dynamics, but only the pressure and thus the forces acting on the plate. The results below are therefore the same, up to a translation, as those for a moving plate in a reference frame fixed at infinity.

The flow is nondimensionalized with respect to the plate length and the parameter a , yielding a characteristic timescale

$$T = \left(\frac{L}{a}\right)^{1/(p+1)}, \quad (2)$$

and flow Reynolds number

$$Re = \frac{L^2}{\nu T} = \frac{a^{1/(p+1)} L^{(2p+1)/(p+1)}}{\nu}, \quad (3)$$

where ν is the kinematic fluid viscosity. The problem is described in nondimensional time t and Cartesian coordinates (x, y) , chosen so that the plate lies on the x-axis, centered at the origin, at $\{(x, 0) | x \in [-1/2, 1/2]\}$. The fluid velocity and scalar vorticity are $(u(x, y, t), v(x, y, t))$ and $\omega(x, y, t)$. The relation between dimensional and nondimensional variables is, for example

$$t = \frac{\hat{t}}{T}, \quad x = \frac{\hat{x}}{L}, \quad U = \frac{\hat{U}T}{L}, \quad \omega = \hat{\omega}T. \quad (4)$$

The nondimensional far field velocity is $(0, t^p)$.

The flow is governed by the incompressible Navier-Stokes equations,

$$\begin{aligned} \frac{D\omega}{Dt} &= \frac{1}{Re} \nabla^2 \omega, \\ \nabla^2 \psi &= -\omega, \end{aligned} \quad (5)$$

$$(u, v) = \nabla^\perp \psi = \left(\frac{\partial \psi}{\partial y}, -\frac{\partial \psi}{\partial x} \right).$$

It is initially irrotational, $\omega(x, y, 0) = 0$, with boundary conditions $\psi = 0$ and $u = 0$ on the plate, and $\psi(x, y, t) \rightarrow \psi_\infty$ as $|(x, y)| \rightarrow \infty$. Here, ψ_∞ is the potential flow that induces the far field velocity, given by the complex potential

$$W_\infty(x, y, t) = t^p \sqrt{\frac{1}{4} - z^2} = \phi_\infty + i\psi_\infty, \quad (6)$$

where $z = x + iy$.

III. NUMERICAL METHOD

The governing equations (5) are solved in a finite rectangular domain in the right half plane, $[0, x_{max}] \times [y_{min}, y_{max}]$, using a time-splitting mixed finite-difference and semi-Lagrangian scheme. The domain in space and time is discretized using a uniform mesh, $\Delta x = \Delta y = h$, with constant timestep Δt , over a given time interval. The solution is advanced from time t_n to t_{n+1} by convecting the current vorticity according to

$$\frac{D\omega}{Dt} = 0 \quad (7)$$

using a semi-Lagrangian scheme; using the updated vorticity to obtain updated interior and boundary streamfunction, velocity and vorticity values; and then solving

$$\frac{\partial \omega}{\partial t} = \frac{1}{Re} \nabla^2 \omega \quad (8)$$

TABLE I. List of parameters in computations: the mesh size h , time step Δt , starting/ending time $t_{\text{start}}/t_{\text{end}}$, computational domain $[0, x_{\text{max}}] \times [y_{\text{min}}, y_{\text{max}}]$, the number of grid points $N_x \times N_y$, the value(s) of p and the Reynolds number Re .

h	Δt	$[t_{\text{start}}, t_{\text{end}}]$	$[0, x_{\text{max}}] \times [y_{\text{min}}, y_{\text{max}}]$	$N_x \times N_y$	p	Re
1/5120	2×10^{-6}	[0, 0.0004]	$[0, 0.55] \times [-0.05, 0.1]$	2816×768	0	500
1/2560	4×10^{-6}	[0, 0.005]	$[0, 0.55] \times [-0.05, 0.1]$	1408×384	0	500
1/1280	5×10^{-5}	[0, 0.1]	$[0, 0.75] \times [-0.125, 0.25]$	960×480	0, 0.5, 1, 2	500
1/640	1×10^{-4}	[0.1, 0.7]	$[0, 0.1] \times [-0.25, 0.75]$	480×480	0, 0.5, 1, 2	500
1/320	2×10^{-4}	[0.7, 3]	$[0, 1.5] \times [-0.25, 2.75]$	480×960	0, 0.5, 1, 2	500
1/160	4×10^{-4}	[3, 4]	$[0, 1.5] \times [-0.5, 5.5]$	240×960	0	500
1/1280	5×10^{-5}	[0, 0.75]	$[-0.1, 0.4] \times [0, 0.5]$	960×640	0.45	6000

using an implicit Crank-Nicolson method. The method is described in detail in Xu & Nitsche¹⁶ and is based on the work in Xu¹⁵.

Table I lists all parameters used in the present computations for various values of p . In several cases, in order to compute the flow to large times, the computations were performed using a fine mesh until some early time, sub-sampling that result and continuing on a coarser mesh, and repeating this process. The time intervals used are indicated in the table. For example, the result for $p = 0$ at $t = 4$ is obtained using $h = 1/1280$ for $t \in [0, 0.1]$, sub-sampling the result at $t = 0.1$ to continue with $h = 1/640$ until $t = 0.7$, etc. The case of $p = 0$ is more difficult to compute in view of the initial singularity at the plate tip discussed in¹⁶. Therefore, finer resolutions are used in this case than for $p > 0$.

In order to compare with laboratory experiment, we also compute particle streaklines by releasing a fluid particle into the flow from the plate tip at each timestep, and evolving it with the fluid velocity.

IV. NUMERICAL RESULTS

A. Vorticity, streamlines, and streaklines for $p = 1$

Figure 2 presents the computed flow evolution for $p = 1$ (constant acceleration) and $Re = 500$. The figure shows vorticity contours (left), streaklines (middle), and streamlines (right) at $t = 0.04, 0.2, 0.5, 1, 1.5, 2$, as indicated. Positive vorticity contours are shown in black, negative ones in a lighter shade of grey. Results are plotted in the right half plane, $x \geq 0$. By symmetry, the vorticity and streamfunction in $x \leq 0$ are of equal magnitude but opposite sign.

Initially, the background flow has zero velocity. As the motion begins, boundary layers of positive vorticity form around the plate, on both the upstream side (below) and downstream side (above). This early vorticity is almost symmetric across the plate at $y = 0$, as can be seen in figure 2 at $t = 0.04$. The corresponding streamlines, in the right column, are also practically symmetric across

the plate. It is noteworthy to remark that this almost symmetric flow regime is not present for the impulsively started case presented in¹⁶. This will be discussed in more detail below.

As time evolves, vorticity upstream from the plate is convected downstream, concentrating near the tip as a vortex that grows in time and breaks the approximate symmetry of the initial boundary layers. At the same time that the vorticity concentrates, a region of recirculating flow forms near the tip. The recirculating region is bounded by the zero level streamline and is seen in figure 2 as early as $t = 0.2$, in the right column. Within the recirculation region and close to the wall, fluid moves in the opposite direction of the background flow, thereby generating a region of opposite signed boundary layer vorticity. This negative wall vorticity appears in the fluid flow at $t \approx 0.1$, and can be seen in figure 2 for all times $t \geq 0.2$. The appearance of the recirculation region near the tip and the associated concentration of vorticity marks the formation of the starting vortex.

The upstream boundary layer vorticity keeps being convected downstream, feeding the starting vortex. As a result, the leading vortex grows in size, and induces more negative vorticity on the plate. The negative vorticity layer thickens and extends toward the axis at $x = 0$, together with the recirculation region. At $t=1$, the downstream wall vorticity is all negative, and separates the plate from the original positive boundary vorticity. The remaining positive boundary vorticity diffuses and vanishes, as seen here at times $t = 1.5, 2$, leaving the starting vortex clearly separated from the original boundary layer vorticity. The negative vorticity near the tip is entrained by the vortex, which grows and convects in the downstream direction.

The streaklines shown in the middle column in figure 2 are computed by releasing fluid particles from the plate tip at each time step, and computing their evolution with the fluid velocity. At any given time, the figure 2 shows the current position of all particles released previously, mimicking what can be visualized in laboratory experiments. The particles rotate around the vortex center, with particles that have been released earlier traveling closer to the center than those released later. This gives the resulting streaklines their spiral shape. We note that

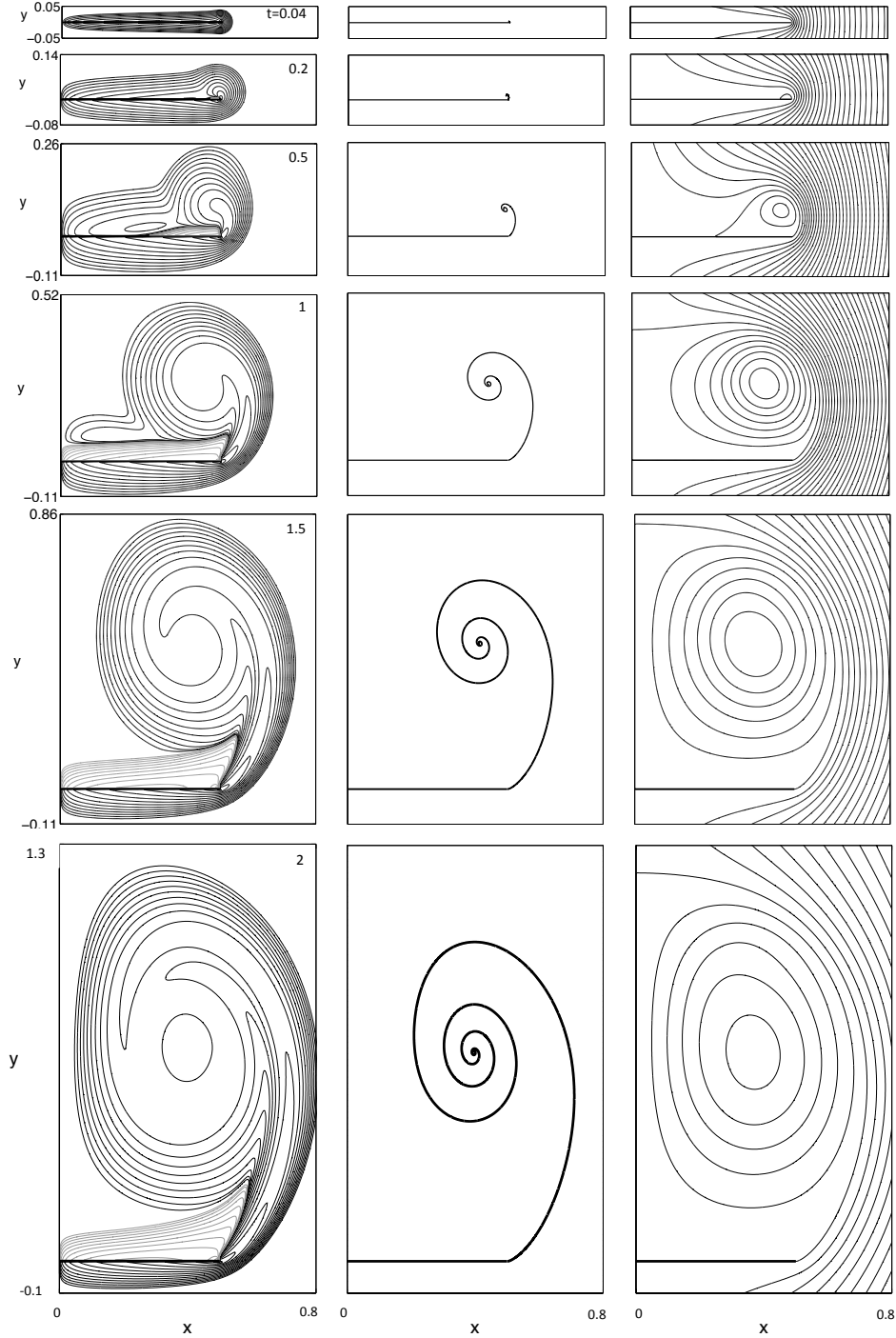


FIG. 2. Vorticity (left), streaklines (middle) and streamlines (right) at $t = 0.04, 0.2, 0.5, 1, 1.5, 2$, for $p = 1$, $Re = 500$. Vorticity contours level are $\pm 2^j$, $j = -5, \dots, 12$.

the tip, which is the point at which the particles are released, is also the point at which the flow vorticity is maximal. The particles thus approximate the convection of the maximum vorticity, and thus approximate the centerline of maximum vorticity in the separated shear layer.

However, the size of the spiral streakline is not representative of the size of the vortex recirculation region.

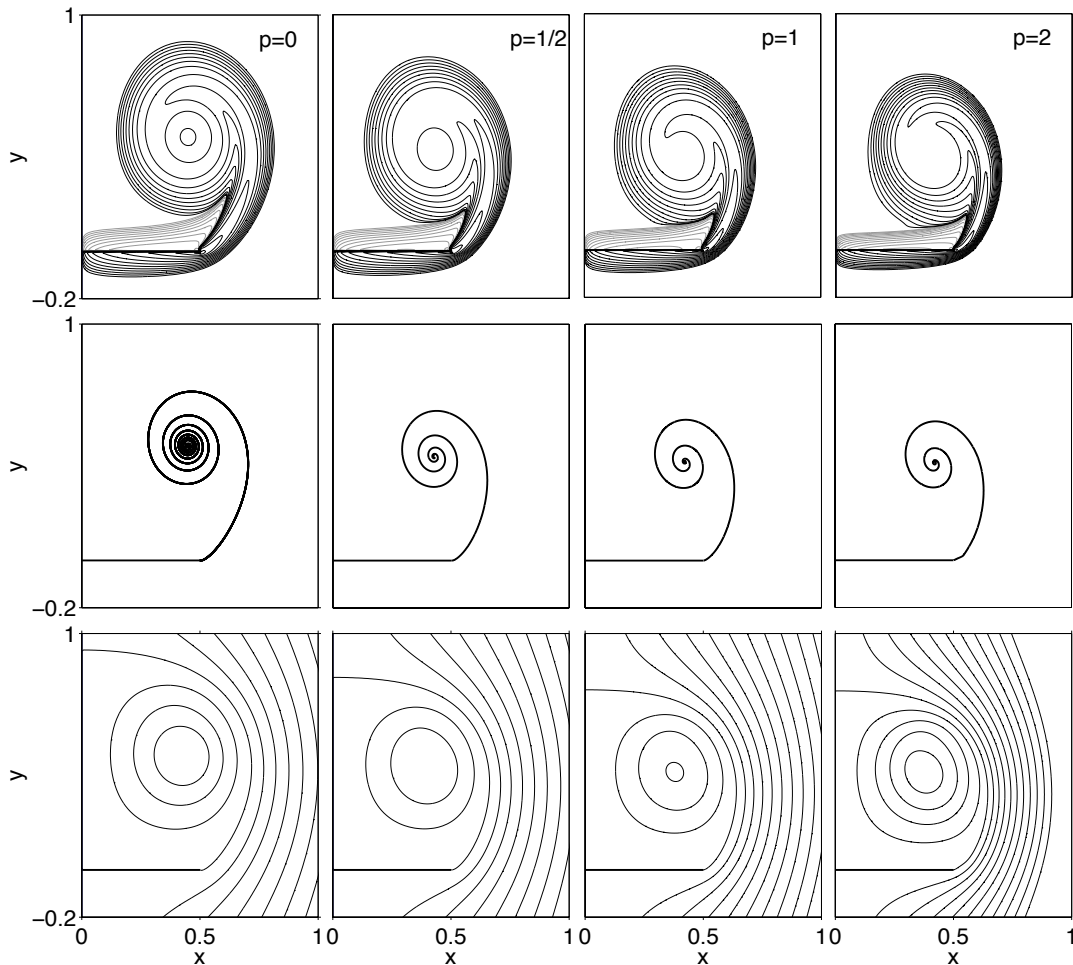


FIG. 3. Vorticity(*top*), streaklines(*middle*) and streamlines(*bottom*) for fixed displacement $d = 1$, and $p = 0, 1/2, 1, 2$, as indicated.

B. Dependence on p at fixed displacement $d = 1$

The parameter p describes the driving velocity $(0, t^p)$ in the far field. In a reference frame fixed at infinity, the plate moves downward with velocity $(0, -t^p)$. The solution for varying p at a fixed time t varies greatly since the plate has travelled significantly different distances $d = \frac{1}{p+1}t^{p+1}$ at equal time t , resulting in vortices of significantly different size. It is more meaningful to compare solutions with varying p at times at which the plate displacement d is equal. All results shown herein that compare the solution for various p are therefore plotted in reference to the displacement d , instead of time t .

Figure 3 compares the vorticity profiles (*top*), streaklines (*middle*) and flow streamlines (*bottom*) at fixed displacement $d = 1$ for all $p=0, 1/2, 1, 2$ computed, as indicated. As p increases, the vorticity contours show that the vortex decreases slightly in size, and the core vorticity becomes more uniform. Furthermore, the wall boundary layer thickness decreases slightly. The vorticity profile as a function of p is more clearly shown in figure 4(a),

which plots the vorticity at $d = 1$ along the vertical line $x = x_m$ through the vorticity maximum (x_m, y_m) in the vortex center, as a function of y , for all p computed. It shows that the profile is flatter near the core for larger values of p . The outermost shear layer turn is stronger for larger p , with larger maximal vorticities, and peaks at a smaller value of y , reflecting the smaller shape seen in the vorticity contours.

The spiral streaklines plotted in the middle row of figure 3 show that as p increases, the spiral size decreases, and the roll-up away from the center is less tight. That is, for larger p , more particles released at early times end up near the spiral center. This is caused by the fact that for larger p , the vortex has travelled less far from the plate at early times. As p increases, the spiral shape is more elliptical and less round. It also leans further to the left, with the line from the spiral center to the plate tip subtending a smaller angle with the plate.

The streamlines plotted in the bottom row in figure 3 show that as p increases, the size of the recirculation region decreases. From the streamline density we deduce that the velocity gradients in the core first decreases as

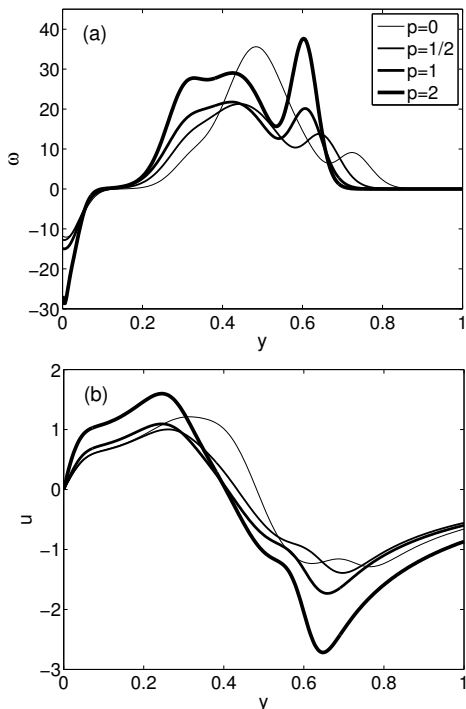


FIG. 4. (a) Vorticity and (b) velocity at $d = 1$ along a vertical line $x = x_m$ through the vorticity maximum, vs. y , for $p = 0, 1/2, 1, 2$, as indicated.

p increases from 0 to $p = 1/2$, but then increase as p increases past $1/2$. Figure 4(b) plots the velocity along $x = x_m$, and shows that this is indeed the case. The profiles also show the decreasing value of y of the point with $u = 0$, near the rotation center.

C. Comparison with laboratory experiments

The most detailed experimental results available for comparison are those of Pullin & Perry¹¹ of flow past a wedge of angle β . Their streakline visualization for their smallest wedge angle used, $\beta = 5^\circ$, is shown in figure 5, left column. The photographs show snapshots of an experiment performed in a rectangular tank, in which water flows from left to right past a planar wedge of height $h = 12.7\text{cm}$ attached to the top of the tank. Near the midsection of the tank, the flow is close to planar. Dye initially lines the walls of the wedge near its tip, and trickles almost vertically downward before the motion begins. The photographs show the position of the dye at the indicated dimensional times after the begin of the fluid flow, for (dimensional) background velocity $U = at^p$, with $p = 0.45$, $a = 0.86 \text{ cm/sec}^{p+1}$. By symmetry, the flow is comparable to flow past a plate with $L = 2h$. At water temperature of 24°C , the corresponding Reynolds number as defined in equation (3) above is $Re = 6621$.

The experimental results are compared with the

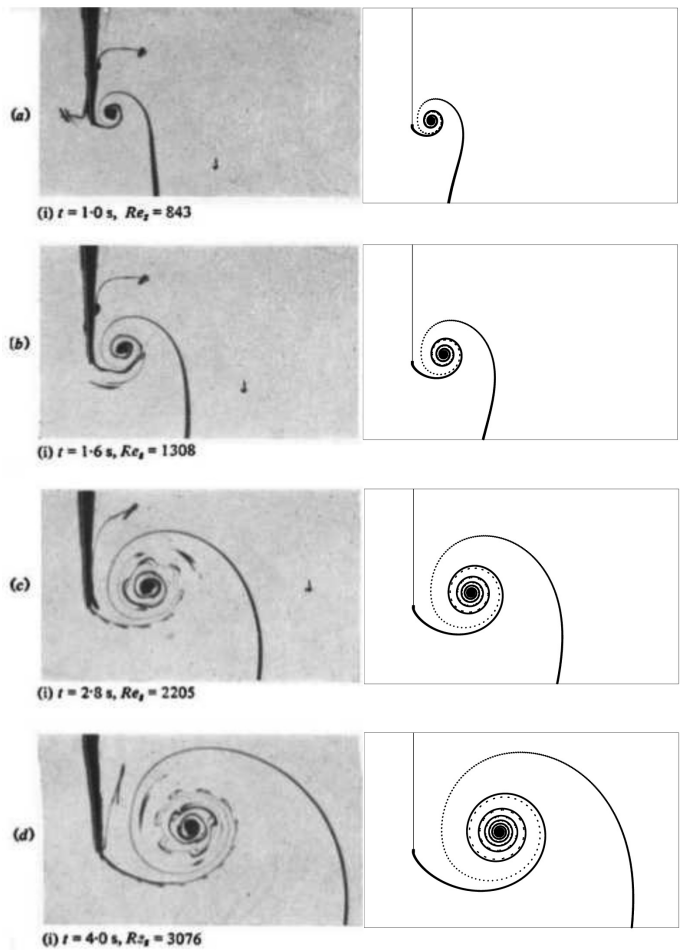


FIG. 5. Left column: Streaklines for flow past a wedge of angle $\beta = 5^\circ$, at $t=1\text{s}$, 1.6s , 2.8s and 4s , for $p = 0.45$ and $Re = 6621$, obtained by Pullin and Perry¹¹ from laboratory experiments (reproduced with permission from the Journal of Fluid Mechanics). Right column: Numerical simulations for flow past a plate ($\beta = 0^\circ$) at the same times, for $p = 0.45$ and $Re = 6000$.

present numerical simulations of flow past a plate ($\beta = 0^\circ$), with $p = 0.45$ and $Re = 6000$. The right column in figure 5 shows the computed streaklines at the nondimensional times corresponding to those shown in the left column, using the timescale in equation (2). The computed results are shown in a rotated frame, for better comparison with the experiments. The figure also plots the position of particles initially placed along a vertical line below the plate (in the rotated frame) to better reproduce the experiment. These particles form the outermost turn of the spiral streakline.

Good agreement between experimental and numerical results is observed for the spiral streakline size, the overall spiral shape, and the spiral center position. The spiral centers will be compared in more detail in section E

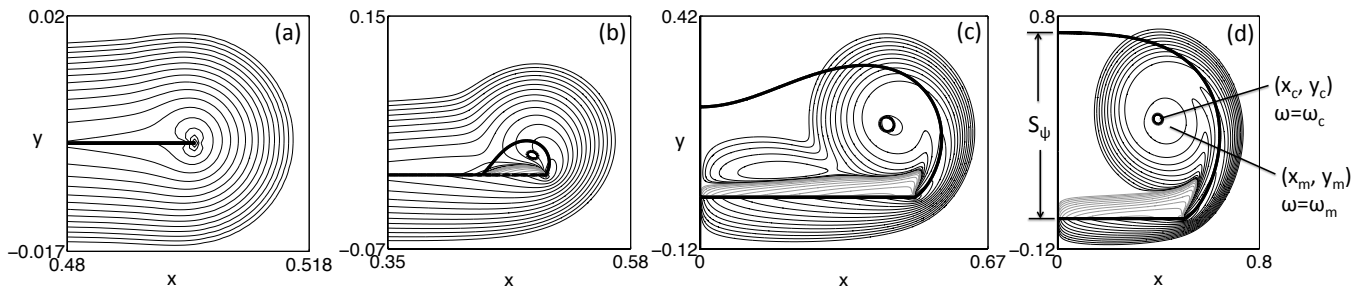


FIG. 6. Four stages in the vorticity evolution, illustrated here for $p = 1/2$, at times (a) $d = 0.00024$ ($t = 0.005$), (b) $d = 0.024$ ($t = 0.11$), (c) $d = 0.310$ ($t = 0.6$) and (d) $d = 0.88$ ($t = 1.2$). Vorticity contours and two streamlines (thick solid lines) are shown. The center of rotation (x_c, y_c) , the position of the vorticity maximum (x_m, y_m) , the corresponding vorticities ω_c and ω_m , and the vortex size s_ψ are indicated in plot (d).

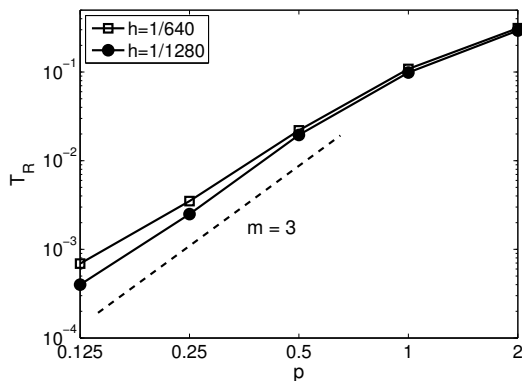


FIG. 7. Duration T_R of the Rayleigh stage, as a function of p , computed with two resolutions $h = 1/1280$ and $h = 1/640$. The dashed line has the indicated slope m .

below. One difference is observed in the spiral turn emanating from the plate tip, which displays small vortices in the experiment, reflecting an instability that is not seen in the computed results at these times. Schneider *et al*¹² give evidence that the shape of a finite thickness plate tip can contribute to these oscillations. Another difference is observed in the outer spiral turn, which has moved further to the right in the experiments than in the computations. This difference may be due to differences in the initial particle positions below the plate, for which the experimental data is not available. It may also be due to differences in the wedge angle between the experiment and the computation, whose effects remains to be studied.

D. Four stages in the vortex evolution

Luchini and Tognaccini⁵ propose four stages in the evolution of the starting vortex. It is interesting to identify them here, as illustrated in figure 6. The figure plots vorticity contours for $p = 1/2$ at an increasing sequence of displacements (see caption). It also plots the level curve

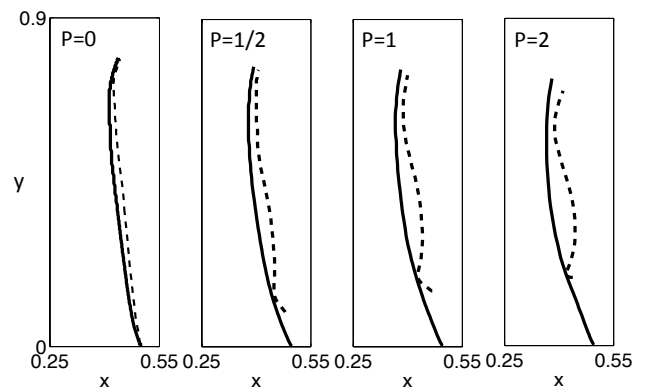


FIG. 8. Trajectories of the rotation center (x_c, y_c) (solid line) and the position of the vorticity maximum (x_m, y_m) (dashed line) for various p , as indicated, for $d \in [0, 3]$.

$\psi = 0$ that bounds the region of recirculating flow, as well as a streamline close to the center of rotation within this region.

In the first stage, referred to as the Rayleigh stage and illustrated in figure 6(a), the vorticity consists of an almost symmetric boundary layer of uniform thickness around the whole plate, without any apparent separated flow. In the second stage a region of recirculating flow has formed near the tip of the plate, containing a well-defined center of rotation, as seen in figure 6(b) and the associated boundary layer of negative vorticity. In this stage the vortex center grows, but does not satisfy scaling laws. Luchini and Tognaccini refer to it as the viscous stage. In the third stage, the self-similar stage, loosely represented by figure 6(c), the vortex center grows closely satisfying the self-similar scaling for inviscid separation in the absence of a plate length scale. The observed scaling behaviour is the subject of the next section. In the last stage, the ejection stage, illustrated in figure 6(d), the vortex departs from the self-similar growth, and the finite plate length noticeably affects the flow.

It is interesting to note that the Rayleigh stage is not

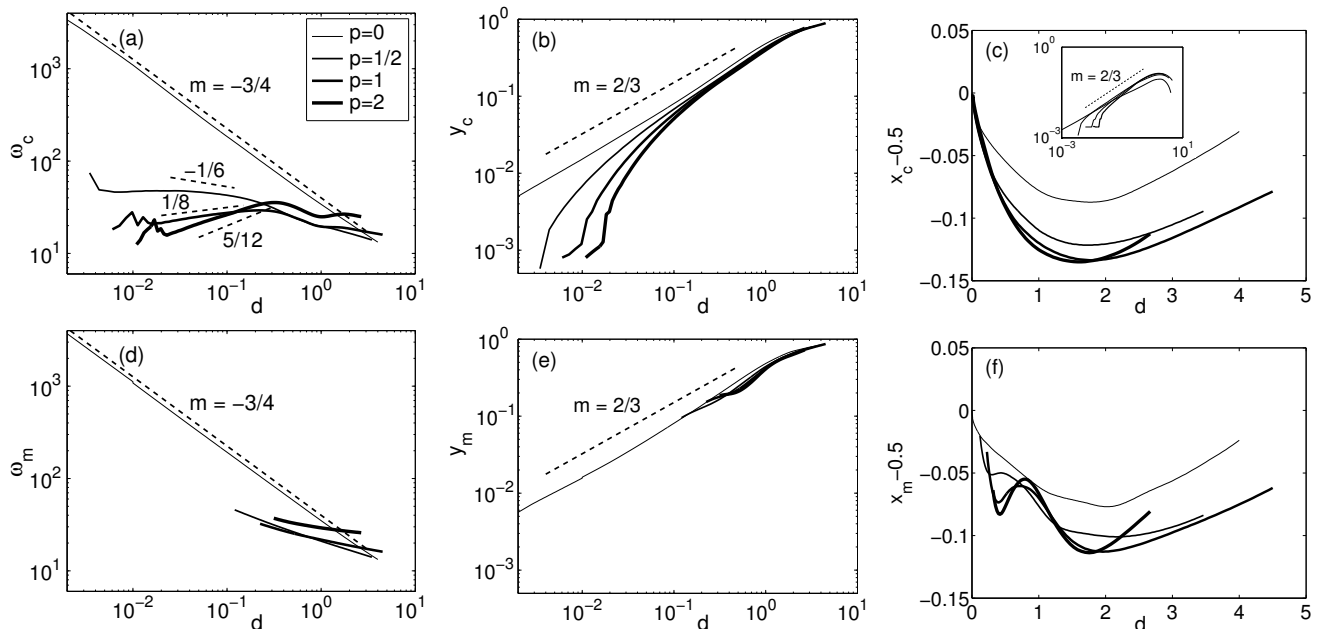


FIG. 9. (a-c) Vorticity and coordinates of the rotation center, *vs.* displacement d . (d-f) Vorticity and coordinates of the core vorticity maximum center, *vs.* displacement d . Results are shown for $p = 0, 1/2, 1, 2$, as indicated in the legend in (a). The dashed lines have the indicated slopes.

observed for the impulsively started flow, $p = 0$. In that case (see also¹⁶), the recirculation region near the plate tip and the associated negative vorticity appear within the first 10-15 timesteps, that is, in time $O(\Delta t)$. Figure 7 plots the duration T_R of the Rayleigh stage, defined by the time at which the recirculation region and negative vorticity first appear, as a function of p . The results were computed using two resolutions, $h = 1/1280$ and $1/640$, as indicated, for $p = 1/8, 1/4, 1/2, 1, 2$. While the convergence is slower for smaller values of p , the interpolating curves appear to converge to

$$T_R \approx 0.15p^3. \quad (9)$$

Thus, T_R grows as p increases, and vanishes for $p = 0$, consistent with our observations.

E. Vortex core trajectory and vorticity

At $t = T_R$, a region of recirculating flow forms with an associated center of rotation, which can be used to define the center of the starting vortex. Alternatively, the vortex center can be defined as the position of the vorticity maximum near its center. However, as can be seen in figure 6(b), at early times when the recirculation region is already well established, no local vorticity maximum has yet formed within the starting vortex. At these early times, the vorticity grows along a curved ridge starting at its maximum value at the plate tip, but the ridge does not develop a local maximum along it until much later. Once the local vorticity maximum appears,

as in figure 6(c,d), it is not at the same location as the center of rotation. We denote the positions of the center of rotation and the vorticity maximum by (x_c, y_c) and (x_m, y_m) , respectively, and the corresponding vorticity at those points by ω_c and ω_m (see figure 6(d)).

Figure 8 compares the trajectory of the rotation center (solid) and the core vorticity maximum (dashed) for $p = 0, 1/2, 1, 2$, computed for displacements $d \in [0, 3]$. The figure shows the trajectories on a one-to-one scale, showing that the vortex travels much faster in the vertical direction away from the plate than in the horizontal direction. The vorticity maximum lies always to the right of the rotation center. The figure shows that as p increases, the vorticity maximum appears later and at a further distance from the plate tip. Furthermore, as p increases, the difference between the two points increases. Finally, while the rotation center travels on a monotonic path inward from the plate tip for most of the interval shown, the vorticity maximum oscillates as it travels downstream. It is possible that such oscillations in the core vorticity is partially responsible for oscillations along the separated shear layer often observed in laboratory experiments and in computations^{3,5,13,14}. However, this issue remains to be investigated.

Figure 9 plots the vortex core vorticity and coordinates as a function of the displacement d , on a logarithmic scale, in order to reveal their scaling behaviour. The top row, figures 9(a,b,c), shows the results ω_c, y_c, x_c for the rotation center, which is the first to form. The bottom row, figures 9(d,e,f), shows the results ω_m, y_m, x_m for the vorticity maximum.

We first discuss the results for core vorticity shown in figures (a,d). As noted in¹⁶, for $p = 0$ the vorticity closely follows the viscous scaling found in flow past a semi-infinite plate, over several decades in time. Consider flow past a semi-infinite plate driven by $\hat{\psi}_\infty = A\hat{t}^p\hat{r}^{1/2}\cos(\theta/2)$, where \hat{r}, θ are the polar coordinates of a point with origin at the plate tip, and A is a dimensional constant. Due to the absence of a plate length scale, it follows from dimensional analysis that the dimensional flow streamfunction has the form

$$\hat{\psi}(\hat{x}, \hat{y}) = A\hat{t}^p(\nu\hat{t})^{1/4}f\left(\frac{\hat{x}}{\sqrt{\nu\hat{t}}}, \frac{\hat{y}}{\sqrt{\nu\hat{t}}}\right). \quad (10)$$

In our case, this scaling can be expected to be a good approximation at early times, as long as the vortex size is small relative to the finite plate length. By taking second derivatives, one finds that the corresponding vorticity scales as $\hat{\omega} \sim A\hat{t}^p(\nu\hat{t})^{-3/4}$. In our nondimensional variables, using $A = L^{1/2}a$, this implies that

$$\omega \sim t^p \left(\frac{t}{Re}\right)^{-3/4} \sim d^{\frac{p-3/4}{p+1}} = d^\alpha, \quad (11)$$

where $\alpha = -3/4, -1/6, 1/8, 5/12$ for $p = 0, 1/2, 1, 2$, respectively. As shown in figure 9(a,d), for $p = 0$ this scaling is observed over a large range of times, both in ω_c and ω_m . For $p > 0$, the scaling is observed in ω_c , but over a much smaller time interval, starting after an initial transition region and ending approximately at $d = 0.2$. Figure 9(d) shows that for $p > 0$, the vorticity maximum ω_m has not even yet formed during those times. It appears only around $d = 0.2$ and does not follow the scaling (11).

Figures 9(b,e) plot the vertical displacements y_c, y_m of the rotation center and the vorticity maximum, respectively, as a function of the plate displacement d , respectively. For $p = 0$, both variables closely satisfy

$$y_c, y_m \sim d^{2/3} \quad (12)$$

over several decades in time, until about $d = 1$. For $p > 0$, the data shows that y_c approximates the same scaling quite well for roughly $d > 0.2$, after an initial transition period. As already noted, the values of y_m do not exist during this transition period. They are in fair agreement with y_c afterwards, as shown in figure 9(e).

Figures 9(c,f) plot the horizontal displacement of the vortex center from the plate tip, $x_c - 0.5$ and $x_m - 0.5$, respectively, as a function of the displacement d . Figure (c) shows that the center of rotation first moves monotonically towards the axis, as could also be seen in figure 8. For larger values of p , it moves further to the left. Approximately around $d = 1.5$, for all p , the vortex turns around and moves outwards. The inset in figure (c) plots $|x_c - 0.5|$ on a logarithmic scale, and shows that during the inward motion, the scaling

$$|x_c - 0.5| \sim d^{2/3}, \quad (13)$$

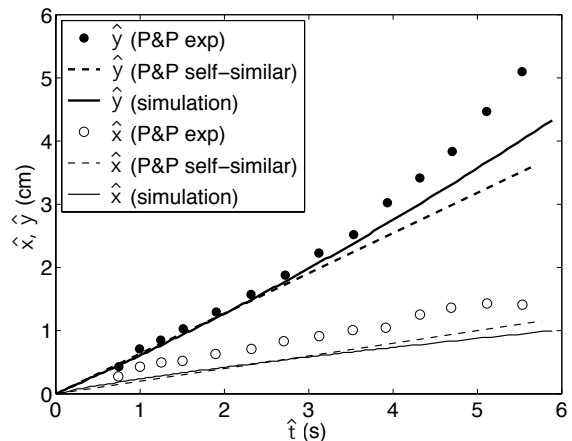


FIG. 10. Comparison of dimensional vortex core coordinates (\hat{x}, \hat{y}) relative to the plate tip, for $p = 0.45$. Experimental results of Pullin & Perry¹¹ ($Re = 6621$), inviscid similarity theory results^{10,11}, and numerical results for the rotation center ($Re = 6000$) are shown.

is approximately satisfied. For $p > 0$, it is satisfied well after an initial transition period. The data for $p = 0$ appears to have a slightly smaller slope, between $2/3$ and $1/2$. The reason for this apparent jump between $p = 0$ and $p = 0.5$ is not quite clear at this point, and needs to be investigated further. The data for x_m , shown in figure 9(f), shows that the vorticity maximum oscillates as it moves inward towards the axis, before it moves back out, as was already observed in figure 8. The oscillation amplitude increases as p increases.

Note that the observed scaling in equations (12,13) is not the one that follows for viscous flow, from the argument leading to (10). Instead, it is the scaling found for inviscid flow in the absence of a length scale, also based on dimensional analysis. This case was considered by Pullin¹⁰, who derives the self-similar scaling for the vortex sheet separation and spiral roll-up at the edge of a semi-infinite plate driven by accelerating background flow, and computes the time-independent self-similar shape using an iterative scheme. His results show that the coordinates of the spiral center satisfy

$$\hat{x}_c + i\hat{y}_c = \Omega_0 \left(\frac{A\hat{t}^{1+p}}{1+p}\right)^{2/3} \quad (14)$$

where the complex number Ω_0 depends little on p . In the dimensionless variables used here, and again making the correspondence $A = L^{1/2}a$, equation (14) is equivalent to equations (12,13).

Next we compare not only the scaling behaviour, but the actual values of the core coordinates with experimental data of Pullin & Perry¹¹ (P&P) and with similarity theory results given therein. Figure 10 plots the dimensional coordinates (\hat{x}, \hat{y}) of the vortex center relative to the plate tip as a function of dimensional time \hat{t} . Consistent with the rest of this paper, \hat{x} refers to the

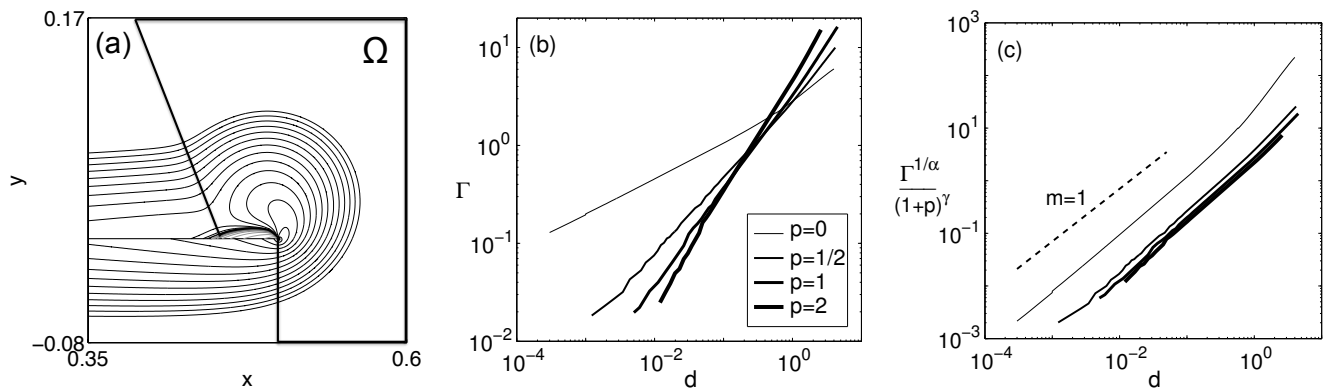


FIG. 11. (a) Sketch showing domain Ω used to define shed circulation Γ , following¹⁶. (b) Γ vs displacement d . (c) $\Gamma^{1/\alpha}/(1+p)^\gamma$ vs d , where $\alpha = \frac{1+4p}{3(1+p)}$, $\gamma = \frac{3p}{1+4p}$. Results are shown for $p = 0, 1/2, 1$ and 2 , as indicated in (b). The dashed line in (c) has the indicated slope.

vortex displacement parallel to the plate, while \hat{y} refers to the displacement normal to the plate. The experimental measurements obtained by P&P (closed and open circles) represent the spiral center of the experimentally observed streakline, for flow past a wedge with $\beta = 5^\circ$. The similarity theory results obtained by Pullin¹⁰ (thick and thin dashed curves) also correspond to flow past a wedge with $\beta = 5^\circ$. The computed results (thick and thin solid curves) denote the dimensional position of the rotation center relative to the plate tip, for a plate with $\beta = 0$, $Re = 6000$, $p = 0.45$. They are dimensionalized appropriately,

$$\hat{x} = L(0.5 - x_c), \quad \hat{y} = Ly_c \quad (15)$$

and shown at dimensional times $\hat{t} = Tt$. The times $\hat{t} \in [0, 6]$ shown in the figure correspond to nondimensional times $t \in [0, 0.58]$, or displacements $d \in [0, 0.31]$. At these times the vortex center still travels towards the axis, with decreasing values of x_c (see figure 9c), that is, increasing values of \hat{x} .

Figure 10 shows that the computed values for the component \hat{y} normal to the plate is in excellent agreement with both the experimental data and similarity theory, for relatively long times $\hat{t} \leq 3$ ($d \leq 0.1$). After this time all three values begin to differ, indicating that the finite plate length and possibly the wedge angle and the physical wall along the centerline begin to affect the results. The computed values remain in between the experimental and the similarity theory results. The computed values for the component \hat{x} tangent to the plate is in less agreement with the experimental data. The experiments show larger deviation from the tip. However, the computed values of \hat{x} , corresponding to $\beta = 0^\circ$, are in surprisingly good agreement with similarity theory results for $\beta = 5^\circ$.

F. Vortex circulation

This section presents the shed circulation Γ as a function of p . No vorticity has separated for $t < t_R$, during which there is a Rayleigh boundary around the whole plate, as shown in figure 6(a). After this time, a region of recirculating flow has formed near the tip which one can associate with a starting vortex. However, the corresponding vorticity is embedded in the boundary layer vorticity, and it is not clear a priori how to define shed vorticity. In order to distinguish separated from attached vorticity, we use the fact that for $t > t_R$, the vorticity contours above the plate develop a point of maximal curvature. These high curvature points closely follow a slant line to the left of the vortex, as shown in figure 11(a). We follow our earlier work^{8,16} and define the separated vorticity to be that enclosed in the region Ω shown in figure 11(a). It includes all vorticity to the right of the tip, and all positive vorticity to the left of the slant line. The negative vorticity attached to the wall is excluded, although it is convected into Ω at later times, when it enters $x \geq 0.5$, such as in figures 6(c,d). This definition has a continuous and natural extension to later times, see¹⁶. The shed circulation is defined to be

$$\Gamma(t) = \int_{\Omega(t)} \omega(\cdot, t) dA. \quad (16)$$

Figure 11(b) plots the circulation Γ , computed with this definition, as a function of the displacement d , for $p = 0, 1/2, 1, 2$, as indicated. Each curve begins at the value of d corresponding to $t = t_R$. For each p , the curves closely follow a straight line in the logarithmic scale shown, indicating a power law behaviour $\Gamma \sim d^\beta$. The slopes β increase with increasing p . They are in fact in close agreement with inviscid similarity theory. Pullin¹⁰ shows that for the self-similar inviscid vortex sheet separation at the edge of a semi-infinite plate, driven by a power law background flow, the separated vortex sheet

circulation Γ_{vsh} satisfies

$$\Gamma_{vsh} \approx J \frac{t^{\frac{1+4p}{3}}}{(1+p)^{1/2}} \quad (17a)$$

where J is only weakly dependent on p . This equation can be rewritten as

$$\frac{\Gamma_{vsh}^{1/\alpha}}{(1+p)^\gamma} \approx J^{1/\alpha} d \quad (17b)$$

where $\alpha = \frac{1+4p}{3(1+p)}$ and $\gamma = 1 - \frac{1}{3\alpha} = \frac{3p}{1+4p}$. To compare the present results for viscous vortex separation with the inviscid similarity theory, figure 11(c) plots $\Gamma^{1/\alpha}/(1+p)^\gamma$, vs the displacement d . The curves for all p are almost parallel and have slope approximately equal to 1, showing that the power law scaling (17b) is closely satisfied, with

$$\Gamma \sim \frac{1}{(1+p)^{1/2}} t^{\frac{1+4p}{3}}. \quad (18)$$

However the constant of proportionality depends significantly on p and increases by a factor of almost 10 as p decreases from $p = 2$ to $p = 0$. The dependence on p increases as p decreases, with a large difference between $p = 0$ and $p = 1/2$, while the results for $p \geq 1/2$ change little.

G. Characteristic sizes

To conclude, this section presents two characteristic sizes of the flow: the boundary layer thickness δ and the size of the recirculation region s_ψ . Figure 12 plots δ^{p+1} vs displacement d , where δ is the vertical thickness of the region below the plate with $\omega \geq 2^{-12}$, at $x=0.25$. The thickness decreases noticeably as p increases. The figure shows that

$$\delta^{p+1} \sim d^{\frac{1}{2}} \quad \text{or} \quad \delta \sim t^{\frac{1}{2}} \quad (19)$$

for approximately $d \in [0, 0.1 - 0.4]$. The scaling holds longer for smaller values of p . The thickness at other values of x is qualitatively similar. Thus, the boundary layer grows as expected, satisfying the viscous scaling of equation 10.

The size of the vortex pair separating at the edge of a finite plate has previously been reported in terms of the quantity s_ψ , defined as shown in figure 6(d) to be the height of the recirculation region on the axis of symmetry along the middle of the plate. Note that this quantity is defined only after the recirculation region has formed and has reached the axis of symmetry, as for example in figure 6(b). Figure 13 plots s_ψ as a function of d , for $p = 0, 1/2, 1, 2$, as indicated. After an initial transition period, the curves for all p approach the same common curve. For approximately $d > 0.5$, this curve closely satisfies

$$s_\psi \sim d^{2/3} \quad (20)$$

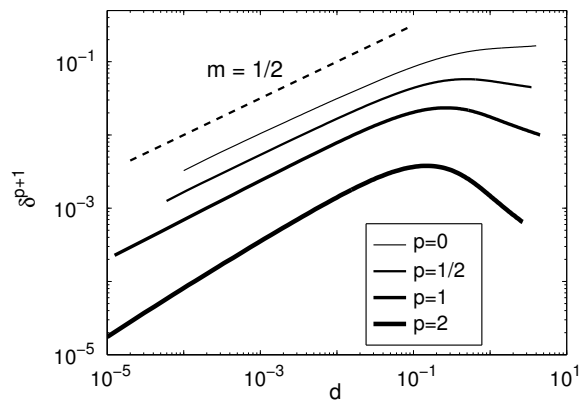


FIG. 12. Boundary layer thickness δ of the region with $\omega \geq 2^{-12}$ at $x = 0.25$, below the plate. The quantity δ^{p+1} is plotted vs displacement d , for $p=0, 1/2, 1$ and 2 , as indicated. The dashed line has the indicated slope.

and is in good agreement with the observations by Taneda & Honji¹³ based on laboratory experiments. The initial transition period is not a viscous or finite plate effect and thus the scaling does not hold asymptotically as $d \rightarrow 0$ in any particular limit. The size does reflect the growth of the vertical vortex displacement y_c , which also scales as $d^{2/3}$.

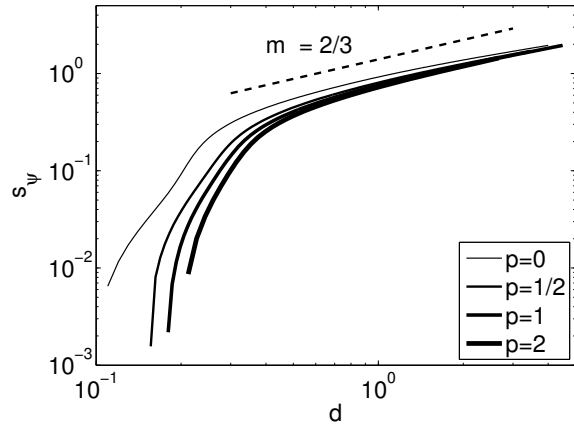


FIG. 13. Vortex size s_ψ vs displacement d , for $p=0, 1/2, 1$ and 2 , as indicated. The dashed line has the indicated slope.

V. SUMMARY

This paper presents a numerical study of viscous flow past a finite flat plate moving with accelerated velocity $U = t^p$ ($\hat{U} = at^{\hat{p}}$) in direction normal to itself. The focus is on the effect of the parameter p , for $p = 0, 1/2, 1, 2$, for fixed value of the Reynolds number, $Re = 500$. All results are computed and presented in a reference frame fixed on the plate. Most results are reported as functions of the plate displacement d , which was found to

more concisely reflect the dependence on p . We report on the vorticity contours, velocity profiles and streaklines at fixed displacement d , and on the evolution of the vortex core trajectory, maximum vorticity, and circulation as functions of d .

At fixed displacement d , the acceleration parameter p affects the vorticity distribution within the core. For example, at $d = 1$, for larger values of p , the outer turns of the shear layer rollup are stronger, and the vorticity profiles near the center are flatter. The spiral roll-up of particle streaklines is more concentrated near the center, with fewer outer turns. The streaklines and the vortex center are in good agreement with available experimental data¹¹ for $p = 0.45$.

Four stages of the vorticity evolution, as proposed by Lucchini & Tognaccini⁵, can be identified. In the initial Rayleigh stage the vorticity consists of an almost uniform layer around the whole plate, including the tip, with no apparent separation. This stage lasts for a time T_R that scales surprisingly well with p , as p^3 , and vanishes as $p \rightarrow 0$. In the second stage a recirculation region has formed near the plate tip, with an enclosed rotation center whose trajectory transitions towards self-similar growth. The third stage is defined by self-similar growth. In the fourth stage the finite plate length significantly affects the flow and the trajectory departs from self-similar. We note that for $p > 0$ the local vorticity maximum within the starting vortex forms much after the center of rotation, and does not grow self-similarly but instead, oscillates in time.

Several scaling laws are observed that follow from dimensional analysis arguments. At early times, when the vortex size is small relative to the plate length, the flow is expected to behave as flow past a semi-infinite plate in which the plate length is absent. For viscous flow, dimensional analysis yields the self-similar streamfunction given by equation (9), from which it follows that length scales and vorticity values behave as

$$L \sim \sqrt{\nu t}, \quad \omega \sim t^p / (\nu t)^{3/4}, \quad (21)$$

respectively. For inviscid flow, dimensional analysis implies that length scales and shed circulation grow as

$$L \sim t^{2(1+p)/3}, \quad \Gamma \sim t^{(1+4p)/3} \quad (22)$$

respectively. For the viscous vortex separation computed here some quantities closely satisfy the viscous scaling, while others are largely independent of viscosity and closely satisfy the inviscid scaling.

For example, the boundary layer thickness closely follows the viscous scaling laws until at least $d = 0.1$. The maximum core vorticity for $p = 0$ is in excellent agreement with the viscous laws as well, for practically the

whole range computed $d \in [10^{-4}, 1]$ (see also¹⁶). For $p > 0$, the viscous scaling is visible for a short time interval only, early on. The vortex center trajectory and circulation on the other hand are largely independent of viscosity and closely follow the inviscid laws after the initial transition time, until relatively large times with $d \approx 1$. As a result, the vortex size, defined as the height of the recirculation region on the axis, also follows the inviscid scaling after it has reached a value comparable to the vertical vortex displacement.

The changes in the computed solutions between $p = 0$ and $p = 0.5$ are much larger than between $p = 0.5$ and $p = 2$. The flow behaviour for $p \in (0, 0.5)$ remains to be studied more closely, as does the dependence on Re for $p > 0$.

- ¹J. D. ANDERSON JR, Ludwig Prandtl's Boundary Layer, *Physics Today* **58** (12), 42–48 (2005).
- ²KADEN, H., Aufwicklung einer unstablen Unstatigkeitsff"ache, *Ingenieur-Archiv Gesellschaft fur Angewandte Mathematik und Mechanik* **2**, 140-179 (1931). (NASA Technical Translation: Curling of an unstable discontinuity surface, NASA-TT-F-14230, 51 p, 1971.)
- ³P. KOUMOUTSAKOS AND D. SHIELS, Simulation of the viscous flow normal to an impulsively started and uniformly accelerated flat plate, *J. Fluid Mech.* **328**, 177–277 (1996).
- ⁴Q. X. LIAN AND Z. HUANG, Starting flow and structure of the starting vortex behind bluff bodies with sharp edges, *Exp. Fluids* **8**, 95–103 (1989).
- ⁵P. LUCHINI AND R. TOGNACCINI, The start-up vortex issuing from a semi-infinite flat plate, *J. Fluid Mech.* **455**, 175–193 (2002).
- ⁶H. J. LUGT, Introduction to Vortex Theory Vortex Flow, Potomac, MD (1996).
- ⁷M. NITSCHKE AND R. KRASNY, A numerical study of vortex ring formation at the edge of a circular tube, *J. Fluid Mech.* **276**, 139–161 (1994).
- ⁸M. NITSCHKE AND L. XU, Circulation shedding in viscous starting flow past a flat plate, *Fluid Dyn. Res.*, to appear (2014).
- ⁹D. PIERCE, Photographic evidence of the formation and growth of vorticity behind plates accelerated from rest in still air, *J. Fluid Mech.* **11**, 460–464 (1961).
- ¹⁰D. I. PULLIN, The large-scale structure of unsteady self-similar rolled-up vortex sheets, *J. Fluid Mech.* **88**, 401–430 (1978).
- ¹¹D. I. PULLIN AND A. E. PERRY, Some flow visualization experiments on the starting vortex, *J. Fluid Mech.* **97**, 239–255 (1980).
- ¹²K. SCHNEIDER, M. PATET-GOY, A. VERGE AND M. FARGE, Numerical simulation of flows past flat plates using volume penalization, *Computational and Applied Mathematics*, DOI: 10.1007/s40314-013-0076-9 (2014).
- ¹³S. TANEDA AND H. HONJI, Unsteady flow past a flat plate normal to the direction of motion, *Journal of the Physical Society of Japan* **30**, 262–272 (1971).
- ¹⁴Z. J. WANG, J. G. LIU AND S. CHILDRESS, Connection between corner vortices and shear layer instability in flow past an ellipse, *Phys. Fluids* **11**, 2446–2448 (1999).
- ¹⁵L. XU, Viscous flow past flat plates, *Ph.D thesis*, University of New Mexico (2012).
- ¹⁶L. XU AND M. NITSCHKE, Numerical study of viscous starting flow past a flat plate, submitted, see also arXiv:1401.3365 [physics.flu-dyn] (2014).